Analysis of an active high-temperature thermal insulation system

S. Maruyama
Institute of Fluid Science, Tohoku University, Sendai, Japan

R. Viskanta
School of Mechanical Engineering, Purdue University, West Lafayette, IN, USA

T. Aihara
Institute of Fluid Science, Tohoku University, Sendai, Japan

An active thermal insulation system consisting of a semitransparent porous medium with gas injection is considered for protecting a structure from intense radiation flux ($\approx 5\,MW\,m^{-2}$). The dependence of the thermophysical properties on temperature and dissociation are taken into account. Air, hydrogen, and dissociating ammonia are considered as representative gases. The effects of dissociating and nondissociating gases on temperature distributions in the gas and solid are examined. The active insulation system reduces the thermal penetration depth as little as a few millimeters in thickness. The present protection system is most effective when the advection–radiation parameter N_c/N_R is larger than 1 or 2.

Keywords: insulation; high temperature; gas injection

Introduction

Thermal protection and insulation are important for cooling of rocket nozzles and reentry vehicles, protection of structures from high-intensity energy beams, and design of furnaces for materials processing. A broad classification of cooling techniques available is presented by Sutton *et al.*[1] Among these techniques, a porous or fibrous medium[2] is one of the most common types of insulation. Recently, a very fine powder layer was introduced by Yarbrough *et al.*[3] and Chu *et al.*[4] for reducing convection and thermal conduction of gas in insulation. At high temperature the thermal conductance of the porous or fibrous media increases, because radiative heat transfer predominates over conduction. Transpiration and mass transfer cooling are well-known techniques for protecting a structure from a high-temperature environment.[5] However, the walls of the system under high temperature are sometimes exposed to high-intensity irradiation, and the surface may be damaged because the vaporized liquid or coolant gas cannot protect the surface from intense irradiation.

Combined conduction, convection, and radiation heat transfer have been studied. A unique high-temperature heat transfer augmentation method using porous media was proposed by Echigo,[6] and an application to a radiant heater was studied by Yoshizawa *et al.*[7] An application of a packed bed for gas heating using solar energy was studied by Flamant *et al.*[8] Previously, we proposed a concept of an active thermal insulation system using a semitransparent porous medium composed of a very fine structure with gas injection.[9] In that study, we used air as a working fluid and assumed that the thermophysical properties of air and the porous medium were constant. The active thermal insulation system can achieve very high performance and thermal protection within a very thin layer of the porous medium. For example, heat flux through the layer can be practically eliminated by keeping the back surface at room temperature with a 5-mm thick layer irradiated by a flux of $1\,MW\,m^{-2}$.

Under very high-intensity irradiation, the injected gas is subjected to a large temperature gradient as it passes through the porous medium. The temperature of the injected gas may increase by as much as 1,000 K. In this situation the thermophysical properties of the gas cannot be treated as temperature independent.

We can take advantage of the endothermic reaction of a dissociating gas for the purpose of increasing advection of heat transfer by the injected gas. The heat capacity of the dissociating gas is extremely large compared to the nondissociating gas, and a decrease in the mass flow rate can be expected from using the dissociating gas. Börsch-Supan *et al.*[10] analyzed endothermic gasification of a solid heated by intense radiation. The energy absorption caused by dissociation of ammonia as it passes through a porous medium was measured by Gorton.[11]

In this article we present an analysis of an active thermal insulation system to study transient heat transfer by combined radiation, convection, and conduction. The temperature dependence of the thermophysical properties of an injected gas, including endothermic reaction of dissociation, are taken into account. The effect of dissociating and nondissociating gases on temperature distributions in the gas and solid is examined. Transient and steady-state behavior of the thermal penetration depth and a generalized correlation of surface temperature for effective protection of the insulation surface is discussed.

Combined heat transfer model

Model equations

We consider a one-dimensional (1-D) layer of a semitransparent high-porosity material as shown in Figure 1. The front surface

Address reprint requests to Professor Viskanta at the School of Mechanical Engineering, Purdue University, West Lafayette, IN 47907, USA.

Received 25 August 1989; accepted 12 January 1990

© 1990 Butterworth–Heinemann

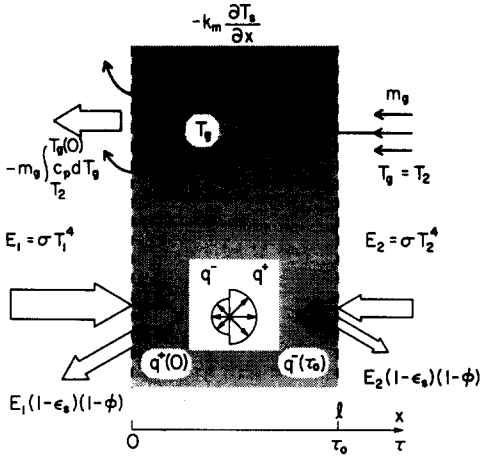

Figure 1 Schematic of the physical model

of the porous layer is exposed to high-intensity thermal radiation, and a low-temperature gas is injected through the back face of the layer. The radiation source in front of the surface is characterized by temperature T_1 and the ambient temperature at the back face is T_2. The mass flux of the gas through the layer is m_g.

In general, the front surface is subjected to convective heat flux. However, we have previously demonstrated that the convective heat flux at the front face affects only the immediate vicinity of the porous layer and does not affect the insulation performance.[9] Hence the convective heat flux at the front face is neglected in the present analysis.

The temperature dependence of all thermophysical properties of the gas and of the thermal conductivity of the porous medium is accounted for in the analysis . The total heat flux through the porous layer is

$$q_t = -k_m \frac{\partial T_s}{\partial x} + q_R - m_g \int_{T_2}^{T_g(x)} c_{pg}\, dT_g \tag{1}$$

where k_m is a function of the solid temperature. As we show in the following section, the porous layer has a very high porosity, and the layer is less than a few centimeters thick. The pressure drop across the layer, while the gas is injected, is estimated to be a few hundred Pascal. Hence the change in pressure in the porous layer is small enough compared to the static pressure (0.1MPa) that the effect of pressure change on the thermophysical properties of the transpiring gas can be neglected. As the layer is thin, the transpiring gas can justifiably be treated as radiatively nonparticipating. The third term on the right-hand side of Equation 1 represents an advective transport of

Notation

A	Advection parameter, Equation 25
A_e	Surface area per unit volume, $1\,m^{-1}$, Equation 4
b, f	Backward and forward scattering fractions
c_{pg}	Specific heat of gas at constant pressure, including enthalpy change caused by dissociation, $J\,kg^{-1}\,K^{-1}$
c_s	Specific heat of porous material, $J\,kg^{-1}\,K^{-1}$
d_p	Equivalent particle diameter of porous media, m
E_b	Dimensionless blackbody emitted flux, Equation 19
E_1, E_2	Radiation fluxes incident on the front and back surfaces from the surroundings, σT_1^4, σT_2^4, $W\,m^{-2}$, Figure 1
h_e	Effective heat transfer coefficient of porous media, $W\,m^{-2}\,K^{-1}$
ΔH	Heat of formation at standard temperature, $J\,mol^{-1}$
i_i	Enthalpy of gas, $J\,kg^{-1}$
i_{mix}	Enthalpy of dissociated gas, $J\,kg^{-1}$, Equation 24
ℓ	Thickness of porous layer, m, Figure 1
k_m, k_g	Thermal conductivity of porous media and gas, $W\,m^{-1}\,K^{-1}$
M_i	Molecular weight of gas, $kg\,mol^{-1}$
m_g	Mass flux of injection gas, $kg\,m^{-2}\,s^{-1}$
n_a	Apparent index of refraction of porous media
Nu_p	Nusselt number based on particle diameter, $h_e d_p/k_g$
N_R, N_c, N_g	Radiation, heat advection, and convection parameter, Equations 10, 11, and 12, respectively
Pr	Prandtl number of gas, $\mu c_{pg}/k_g$
q^+, q^-	Forward and backward radiation fluxes, $W\,m^{-2}$
q_R	Radiation flux, $q^+ - q^-$, $W\,m^{-2}$
q_t	Total heat flux through porous media, $W\,m^{-2}$, Equation 1
Q, Q^+, Q^-, Q_R	Dimensionless heat flux, $Q=q/(E_1-E_2)$, $Q^+=q^+/(E_1-E_2)$, $Q^-=q^-/(E_1-E_2)$, $Q_R=q_R/(E_1-E_2)$
Re_p	Particle Reynolds number, $m_g d_p/\mu$
T_1, T_2	Radiation source temperatures at the front and back surface, K, Figure 1
T_g	Mixing cup temperature of gas, K
T_s	Temperature of porous media, K
t	Time, s
t^*	Dimensionless time, Equation 8
X	Dimensionless length, x/ℓ
x_p	Thermal penetration depth, m, Equation 26

Greek symbols

ε_s	Surface emissivity of solid cross section at boundary, Figure 1
θ_s, θ_g	Dimensionless temperatures of porous media and gas, $(T_s-T_2)/(T_1-T_2)$, $(T_g-T_2)/(T_1-T_2)$
μ	Viscosity of gas, Pa s
ξ_i	Mole fraction of gas
ρ_s, ρ_g	True density of porous material and density of gas, $kg\,m^{-3}$
σ	Stefan–Boltzmann constant, $W\,m^{-2}\,K^{-4}$
σ_e	Extinction coefficient, $1\,m^{-1}$
ϕ	Porosity of porous media
ω_o	Single scattering albedo of porous media
τ	Optical depth, $\sigma_e x$
τ_o	Optical thickness, $\sigma_e \ell$, Figure 1

Subscripts

1, 2, 3	Values of NH_3, H_2, and N_2, respectively
$[\,]_{T_r}$	Fluid properties evaluated by the temperature T_r

energy by the transpired gas. A special treatment of c_{pg} is required when the gas is dissociating, which we discuss in the following subsection.

Order of magnitude analysis of the storage terms in the energy equations for gas and the solid matrix reveals that the storage term in the energy equation for the gas can be neglected in comparison to advection or convection. The governing energy equations for the porous solid and the gas can be expressed as

$$(1-\phi)\rho_s c_s \frac{\partial T_s}{\partial t} = \frac{\partial}{\partial x}\left(k_m \frac{\partial T_s}{\partial x}\right) - \frac{\partial q_R}{\partial x} + m_g c_{pg} \frac{\partial T_g}{\partial x} \tag{2}$$

$$-m_g c_{pg} \frac{\partial T_g}{\partial x} = A_e h_e (T_s - T_g) \tag{3}$$

where A_e and h_e are the effective surface area per unit volume and the heat transfer coefficient of the gas and the solid, respectively. We assume that the solid matrix can be represented by a packed bed of spherical monodisperse particles of diameter d_p. Then,

$$A_e = \frac{6(1-\phi)}{d_p} \tag{4}$$

The empirical correlation proposed by Huber and Jones[12] is adopted for estimation of the heat transfer coefficient of the porous media; that is

$$\mathrm{Nu_p} = 0.054\mathrm{Re_p^{1.48}} \tag{5}$$

We assumed that the mean free path of the gas molecules is much smaller than the particle size. We showed previously[9] that there is a large difference between the gas and solid temperatures. Important in such a case, is choosing an appropriate reference temperature at which the thermophysical properties appearing in Equation 5 are evaluated for estimating the heat transfer coefficient.[13]

For the case of forced convection heat transfer in a duct, the mixing cup temperature of fluid is generally used for a reference temperature.[14] The heat transfer characteristics can be correlated well by using the mixing cup temperature, even for the case of natural convection in the ducts with an imposed constant heat flux.[15] Thus the mixing cup temperature may be appropriate for use in evaluating the heat transfer coefficient in Equation 5. Note that the mixing cup temperature of the gas is identical with T_g in Equations 2 and 3.

Introducing the dimensionless parameters θ_s, θ_g, X, and Q_R, we can rewrite the energy Equations 2 and 3 as

$$\frac{\partial \theta_s}{\partial t^*} = N_k \left(\frac{\partial \theta_s}{\partial X}\right)^2 + \frac{\partial^2 \theta_s}{\partial X^2} - N_R \frac{\partial Q_R}{\partial X} + N_c \frac{\partial \theta_g}{\partial X} \tag{6}$$

$$\frac{\partial \theta_g}{\partial X} = -N_g(\theta_s - \theta_g) \tag{7}$$

where

$$t^* = \left[\frac{k_m}{\rho_s c_s}\right]_{T_s} \frac{t}{(1-\phi)\ell^2} \tag{8}$$

$$N_k = \left[\frac{1}{k_m}\frac{\partial k_m}{\partial \theta_s}\right]_{T_s} \tag{9}$$

$$N_R = \left[\frac{1}{k_m}\right]_{T_s} \sigma(T_1+T_2)(T_1^2+T_2^2)\ell \tag{10}$$

$$N_c = \left[\frac{1}{k_m}\right]_{T_s} [c_{pg}]_{T_s} m_g \ell = \left[\frac{1}{k_m}\right]_{T_s} [k_g \mathrm{PrRe_p}]_{T_s} \frac{\ell}{d_p} \tag{11}$$

$$N_g = 6(1-\phi)\frac{\ell}{d_p}\left[\frac{\mathrm{Nu_p}}{\mathrm{PrRe_p}}\right]_{T_s} \tag{12}$$

These parameters are functions of the solid temperature T_s and the gas temperature T_g.

The initial and boundary conditions are

$$-\frac{\partial \theta_s}{\partial X} = \frac{\ell(1-\phi)}{k_m(T_1-T_2)} \varepsilon_s \sigma [T_1^4 - T_s^4(0)] \quad \text{at } X=0 \tag{13}$$

$$-\frac{\partial \theta_s}{\partial X} = \frac{\ell(1-\phi)}{k_m(T_1-T_2)} \varepsilon_s \sigma [T_s^4(\ell) - T_2^4] \quad \text{at } X=1 \tag{14}$$

$$\theta_g = 0 \quad \text{at } X=1 \tag{15}$$

$$\theta_g = \theta_s = 0 \quad \text{for } t^*=0 \tag{16}$$

As far as radiative transfer is concerned, many approximate methods have been proposed for predicting the radiative transfer in dispersed media. Menguc and Viskanta[16] assessed the validity of several different methods by comparing the prediction with the exact solution. They found that the two-flux approximation yields sufficiently accurate results. Consequently, we use the two-flux approximation in our analysis of the radiative heat transfer. The dimensionless forms of the transport equations are

$$\frac{1}{2}\frac{dQ^+}{d\tau} = -(1-f\omega_o)Q^+ + \omega_o b Q^- + (1-\omega_o)E_b \tag{17}$$

$$-\frac{1}{2}\frac{dQ^-}{d\tau} = -(1-f\omega_o)Q^- + \omega_o b Q^+ + (1-\omega_o)\mathrm{E}_b \tag{18}$$

where

$$E_b = \frac{n_a^2 \sigma T_s^4}{(E_1 - E_2)} \tag{19}$$

and

$$\frac{\partial Q_R}{\partial X} = 2\tau_o(1-\omega_o)(-Q^+ - Q^- + 2E_b) \tag{20}$$

In our analysis, we adopted the effective refractive index n_a as originally derived by Maxwell–Garnett[17] for the refractive index of the porous material.

For simplicity, we assume that the radiative properties of the porous material is independent of temperature and gray. We adopted the same boundary conditions as the previous report[9] for the radiative transfer:

$$Q^+ = \{\phi + \varepsilon_s(1-\phi)\}\frac{E_1}{E_1 - E_2} \quad \text{at } \tau = 0 \tag{21}$$

$$Q^- = \{\phi + \varepsilon_s(1-\phi)\}\frac{E_2}{E_1 - E_2} \quad \text{at } \tau = \tau_o \tag{22}$$

We solved the Equations 6, 7, 17, and 18 numerically using a finite difference method with an iterative procedure that is basically the same as reported in Reference 9, except that the thermophysical properties in Equations 8–12 are functions of temperature rather than constants.

Thermophysical properties of dissociating gas

A dissociating gas might be particularly effective at high-temperature conditions. At very high temperature use of a dissociating gas that has a large heat of formation may be particularly advantageous. However, a review of the literature revealed that no work has been done on using such gases in the thermal protection method considered here.

As a concrete example, let ammonia at 1 atm be the working gas. Although ammonia has a rather low dissociation temperature, its thermophysical and thermodynamic properties are

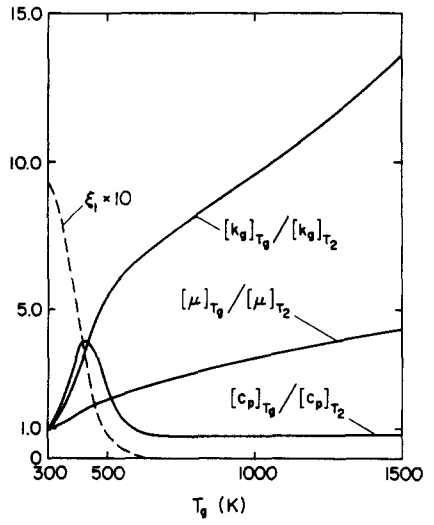

Figure 2 Temperature dependence of thermophysical properties and the mole fraction of dissociating ammonia at an equilibrium state; each property normalized with respect to the value at 300 K

well established. Air and hydrogen at 1 atm are also considered as examples of nondissociating working gases.

The endothermic energy of dissociating ammonia is strongly dependent on the mole fraction of the gas mixture resulting from the chemical reaction. The mole fraction is dependent not only on temperature but also on the reaction rate. The reaction rate is also strongly affected by the catalyst and the configuration of the porous medium. For simplicity we consider two extreme cases: (1) the case for pure ammonia without dissociation (NH_{3p}); and (2) the case for the ammonia at an equilibrium state (NH_{3e}). As already discussed, the pressure drop in the porous layer is relatively small. Then, the mole fraction of ammonia at the equilibrium state is a function of temperature only, and the other thermophysical properties can be calculated relatively easily. Although assuming that ammonia is in an equilibrium state at low temperature is unrealistic, actual dissociation takes place between the two limiting cases. The idealizations presented reduce the complexity of the problem, because the reaction rate depends on many parameters, and the simplification gives some insight into the effect of dissociation. The thermophysical properties of pure ammonia are obtained from the literature.[18]

The mole fractions ξ_i of NH_3, H_2, and N_2 are calculated by:

$$P_t K_p = \frac{\xi_1}{\xi_2^{3/2}\xi_3^{1/2}} \tag{23}$$

where P_t is the total pressure of the gas, and the equilibrium constant K_p can be found in the literature.[19] Then, the enthalpy at an equilibrium state can be calculated from:

$$i_{mix} = \sum_{i=1}^{3} \frac{\xi_i M_i i_i}{M_m} - \Delta H\left(\frac{1}{M_1} - \frac{\xi_1}{M_m}\right) \tag{24}$$

where $M_m = \sum_{j=1}^{3} M_j \xi_j$. As i_{mix} is a function of temperature only, the specific heat of the gas mixture at the equilibrium state can be defined by differentiating the enthalpy. Note that the specific heat in our definition is not the sum of the specific heats of each component gas but includes the change in the heat of formation and that the pressure drop across the porous layer can justifiably be neglected. The calculated enthalpy and the specific heat of ammonia at an equilibrium state is identical to the values reported in Reference 20. The viscosity and thermal conductivity of the dissociated gas mixture can be approximated by Wilke's semiempirical formula.[21]

The thermophysical properties of air,[22] hydrogen,[18] and pure ammonia without dissociation[18] are available in the literature and are not repeated here. Suffice it to say that both k_g and μ show a monotonic increase with temperature, c_{pg} for both air and hydrogen is almost constant for $T_g < 2000$ K, and c_{pg} for ammonia increases with temperature. Variations in thermophysical properties and the mole fraction of ammonia at an equilibrium state are shown in Figure 2. The thermophysical properties were normalized with respect to the values at 300 K. Note that the thermophysical properties vary greatly with temperature for the case of dissociating ammonia at an equilibrium state. There is a very large change in c_{pg}, and there is a maximum in the specific heat at about $T_g = 450$ K. At that temperature the dissociation rate increases greatly with increasing temperature. At $T_g > 700$ K, c_{pg} is almost constant, because dissociation is complete in this temperature range. The absolute value of c_{pg} in this region is approximately the same as that of pure ammonia. Increases in the other properties with temperature are quite large compared to those in other gases.

Results and discussion

Effect of thermophysical properties on heat advection parameters

Numerous publications in the literature are concerned with radiative properties of porous or fibrous material (for example, Kurosaki *et al.*[23]). Matthews *et al.*[24] estimated both thermal and radiative properties of high-temperature porous zirconia from their experimental results, and the values have been used in the analysis by Matthews *et al.*[2] A more complete and recent discussion of radiative properties of dispersed media is available.[25] The data for a porous zirconia[24] is used for the thermophysical and radiative properties listed in Table 1. The porosity, ϕ, is assumed to be 0.9 and particle diameter d_p to be 100 μm. For most cases in our numerical analysis, we chose the temperature of the radiation source in front of the face to be 3000 K. We did so in order to obtain an incident flux of approximately of 5 MW m^{-2} at the front face. We chose a back face temperature T_2 of 300 K.

The effect of temperature dependence of the thermophysical properties on the heat advection parameter N_c is illustrated in Figure 3. The mass flux of the gas is fixed and T_g is changed from 300 K to 1,500 K through the 10-mm thick porous layer. We assumed that T_s is given by the relation $\theta_s = 2\theta_g$. The value of N_R is also plotted as a reference. The values of N_c decrease slightly with increasing T_g and T_s, except for ammonia in an equilibrium state. Recalling the definition of N_c and noting that it is a function of c_{pg} and k_m only, we ascribe the change in N_c mainly to the increase in k_m. However, the absolute values of

Table 1 Thermophysical and radiation properties of porous zirconia

Thermophysical properties
$c_s = 1.75 \times 10^3$ J kg^{-1} K^{-1}
$\rho_s = 5.60 \times 10^3$ kg m^{-3}
$\phi = 0.9$ (assumed)
$d_p = 100\ \mu$m (assumed)
$k_m = 7.0 \times 10^{-2} + 4 \times 10^{-5}(T_s - 300)$ W m^{-1} K^{-1}
Radiation properties
$\sigma_e = 8.969 \times 10^3$ m^{-1}
$b = 0.2506$
$\omega_o = 0.99$
$n_s = 1.05$
$\varepsilon_s = 0.35$

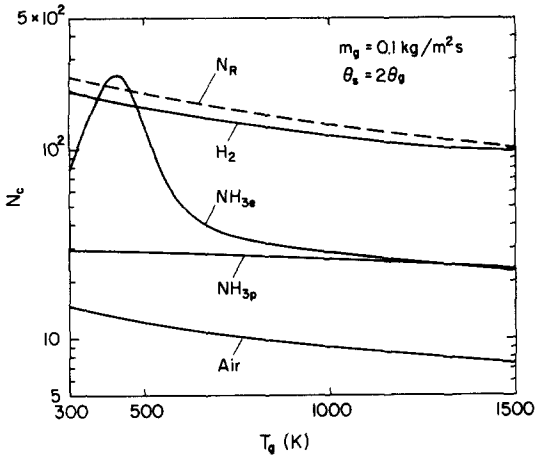

Figure 3 Variation of the heat advection parameter N_c for various types of gases ($T_1=3{,}000$ K, $T_2=300$ K, $\ell=10$ mm, $m_g=0.1\,\mathrm{kg\,m^{-2}s^{-1}}$)

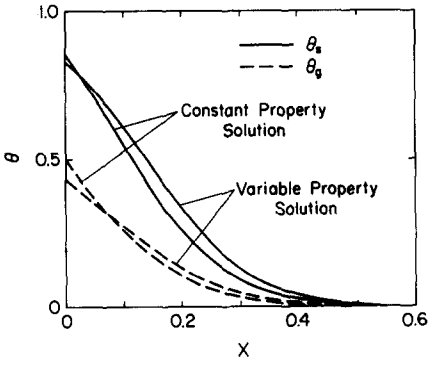

Figure 4 Comparison of temperature distributions of gas and porous solid for constant-property and variable-property solutions (air, $T_1=3{,}000$ K, $T_2=300$ K, $\ell=10$ mm, $m_g=0.5\,\mathrm{kg\,m^{-2}s^{-1}}$)

N_c reveal large differences from each other. For example, the variation of N_c for NH_{3e} shows very large differences from the other gases. It has a maximum point that corresponds to the maximum point of c_{pg}. When dissociation is complete at $T_g>700$ K, the parameter N_c for NH_{3e} is similar in value to that for pure ammonia. The difference in N_g between gases is not as large as that for N_c.

Effect of temperature dependence of thermophysical properties

Temperature distributions in the solid and gas—with variable and constant thermophysical properties—are compared in Figure 4. We chose air as a working gas and the mass flux, m_g, as $0.5\,\mathrm{kg\,m^{-2}s^{-1}}$. The thermophysical properties for the constant-property case are taken to be those at T_2 ($=300$ K). Although the thermophysical properties of air vary greatly over the temperature range considered, the constant-property solution shows surprisingly good correspondence with the variable-property results. The main reason is that the parameters N_c and N_g do not change markedly across the layer. This agreement demonstrates that the constant-property solution yields reasonably reliable results if the mass flux is fixed and the variation in the specific heat of the gas with temperature is not as large as is the case for a dissociating gas.

Figure 5 shows steady-state temperature distributions in the solid and gas for nondissociating gases in which the thermophysical properties are considered to be temperature dependent. The temperature distribution in the solid without gas injection is also plotted ($m_g=0$) for comparison. The active insulation system with gas injection greatly reduces penetration thickness and back-face temperature compared to those of a conventional insulation system without gas injection.

In terms of the same mass flux, the temperatures for hydrogen injection are much smaller than those for air. Hydrogen effectively decreases both solid temperature and thermal penetration thickness with constant mass flux. The large difference in temperature distribution results mainly from the large difference in the heat advection parameter N_c for each gas, as shown in Figure 3.

Temperature distributions in the gas and solid for ammonia are presented in Figure 6. The two limiting cases of nondissociating pure ammonia (NH_{3p}) and ammonia in an equilibrium state (NH_{3e}) are shown. The temperatures for NH_{3e} are smaller than those for NH_{3p}. The decrease in the gas temperature for NH_{3e} is particularly remarkable because of the much larger value of c_{pg}, compared to that for NH_{3p}, resulting from energy absorption by dissociation. However, the difference in the solid temperature is not as large as that in the gas temperature. The front-surface temperature of the solid for NH_{3e} transpiration shows a slightly smaller value than that for NH_{3p}. Comparison of Figures 5 and 6 reveals that the surface temperature for transportation of NH_{3e} is larger than that for H_2 for the same mass flux.

Examination of the large difference in temperatures for a fixed mass flow rate and the variation in parameter N_c in Figure 3 reveals that the temperature difference is primarily the

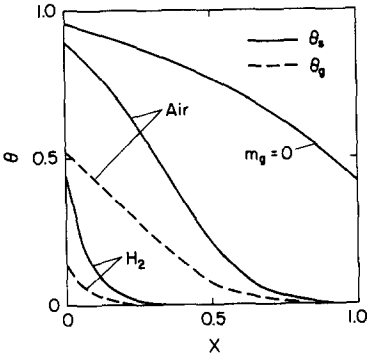

Figure 5 Comparison of temperature distributions between air and hydrogen for the same mass flux ($T_1=3{,}000$ K, $T_2=300$ K, $\ell=10$ mm, $m_g=0.2\,\mathrm{kg\,m^{-2}s^{-1}}$)

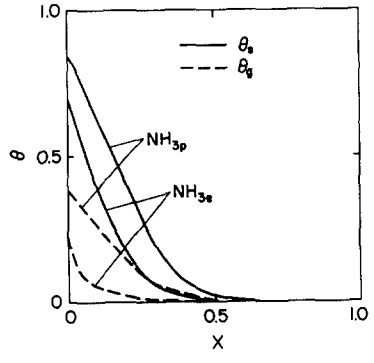

Figure 6 Temperature distributions for pure ammonia without dissociation (NH_{3p}) and dissociating ammonia at an equilibrium state (NH_{3e}) ($T_1=3{,}000$ K, $T_2=300$ K, $\ell=10$ mm, $m_g=0.2\,\mathrm{kg\,m^{-2}s^{-1}}$)

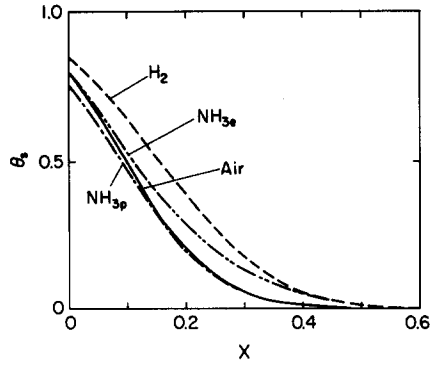

Figure 7 Temperature distributions of porous solid for different gases with fixed advection parameter $A=[PrRe_p k_g/k_m]T_2=1.0$ ($T_1=3{,}000$ K, $T_2=300$ K, $\ell=10$ mm)

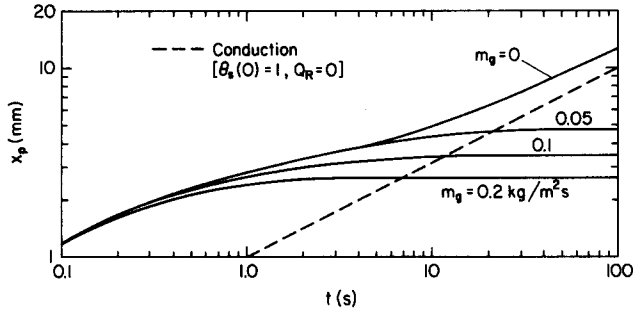

Figure 8 Transient propagation of thermal penetration depth with mass flux of hydrogen ($T_1=3{,}000$ K, $T_2=300$ K)

result of the difference in N_c. Inspection of the advection parameter N_c defined by Equation 11 reveals that the parameters and properties that depend on the thermophysical properties are Pr, Re_p, k_g, and k_m. Hence, in order to correlate the temperatures for various gases, we introduce an advection parameter defined as

$$A=\left[\frac{PrRe_p k_g}{k_m}\right]_{T_2} \tag{25}$$

For an advection parameter of $A=1.0$ for various gases, we plotted the temperature distributions in the solid in Figure 7. The corresponding mass flux for air, H_2, NH_{3p}, and NH_{3e} are 0.68, 0.049, 0.33, and 0.14 kg m^{-2} s^{-1}, respectively. The temperature distributions correlate rather well, compared to the case of fixed mass flux in Figures 5 and 6, although there is some deviation near $X=0.2$. Note that the mass flux for H_2 is 14 times smaller than for air for the same advection parameter, A. So far as nondissociating gases are concerned, the specific heat of monoatomic, diatomic, and polyatomic gases can be approximated roughly as $3R/2M$, $5R/2M$, and $3R/M$, respectively, where R is the universal gas constant and M is the molecular weight of gas. For the same types of gases (monoatomic, diatomic, and polyatomic), the advection parameter A is nearly equal for the same molar flux, i.e., superficial velocity of injected gas. The ratio of mass flux between air and hydrogen for $A=1$ is almost equal to the inverse ratio of the molecular weights.

Transient and steady-state depth of thermal penetration

As shown in our previous work,[9] the active thermal insulation system can eliminate the heat flux through the layer completely within the small thickness. Also, the temperature of the solid at the back face remains very low. In order to achieve the desired performance, a finite thickness is required, even though the thickness is very small compared to that of a conventional insulation system. We previously had pointed out that the thermal penetration depth is important for both insulation performance and transient behavior of the system.[9] In the present analysis, the thermal penetration depth x_p is defined as the thickness at which the solid temperature is reduced to $\theta_s=0.01$, i.e.,

$$\theta_s=0.01 \qquad \text{at } x=x_p \tag{26}$$

In the discussion of Figure 4, we showed that there is only a small difference between the constant-property solution and the variable-property solution. Of the four gases considered, hydrogen performed best, in terms of the same mass flux. Hence we chose H_2 as the injected gas and assumed constant thermophysical properties (evaluated at $T_2=300$ K) for the numerical analysis. The thickness of the porous media chosen should produce sufficient attenuation in the temperature of the solid and the heat flux at the back face.

Transient propagation of the thermal penetration depth is shown in Figure 8 for various mass fluxes of the injected gas. The penetration depth without gas injection and that for pure conduction are also shown for comparison. For the case of the pure conduction model, the surface temperature at $X=0$ was assumed to be $T_1=3{,}000$ K, and x_p was obtained from an analytical solution.

At the initial stages of heating ($t<0.3$ s), the penetration depth for various mass fluxes coincides with the one without gas injection. Initially, radiative heat transfer and the effect of the heat capacity of the porous medium predominate over advective transport. Moreover, the penetration depth at the initial heating stage is much larger than that for pure conduction, because the radiative flux propagates instantaneously, and the porous media is heated by incident radiation flux. As time increases, the penetration depth with gas injection reaches a finite value. However, the depth without gas injection increases monotonically with time, and gradually approaches the value predicted by the pure conduction model. The penetration depth with gas injection reaches steady-state values for very small thicknesses. However, the penetration depth for the case of no gas injection and pure conduction never reaches steady state.

The steady-state penetration depth for various mass fluxes is plotted in Figure 9. The characteristic particle diameter d_p (100 μm in Table 1) varies from 10 μm to 1,000 μm (1 mm). The characteristic particle size affects greatly the convective heat transfer parameter N_g defined by Equation 12, and the smaller the d_p, the larger N_g becomes. The thermal penetration depth decreases with the decrease in the particle size but increases

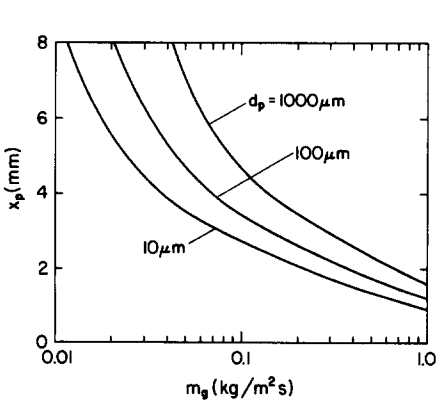

Figure 9 Steady-state thermal penetration depth for different mass flux and particle sizes of porous media d_p (H_2, $T_1=3{,}000$ K, $T_2=300$ K)

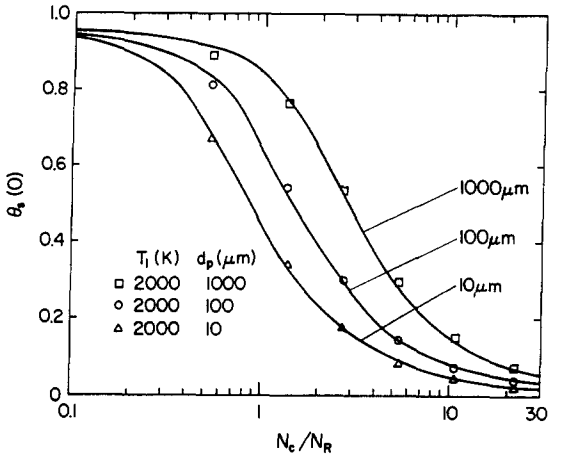

Figure 10 Dependence of solid temperature at the front face on the advection–radiation parameter, N_c/N_R, for various source temperatures T_1 (H_2, $T_2=300$ K); the parameter given is a perturbation from the standard condition: $T_1=3{,}000$ K, $d_p=100\,\mu$m, $\sigma_e=9\times10^3\,m^{-1}$

abruptly for small mass flux. For large mass fluxes the penetration depth x_p is insensitive to both d_p and m_g. However, the penetration depths differ greatly with d_p for small mass fluxes. As shown in Figure 9, the thermal penetration thickness is less than 3 mm for $m_g>0.1\,kg\,m^{-2}\,s^{-1}$ and $d_p=10\,\mu$m. The heat flux through the porous layer can be eliminated within the small layer thickness. Figure 9 shows how insulation thickness can be reduced by injecting hydrogen.

Predicting surface temperature

In the present active thermal insulation system, protection of the structural surface from intense radiation flux is important, as is the thickness of the porous layer. The surface temperature of the porous medium is a function of irradiation, gas injection velocity, and radiative and thermophysical properties of the gas and the porous medium. Although estimating the surface temperature by a simple relation is difficult, lowering the surface temperature efficiently with minimum gas injection is important.

Considering steady-state conditions with constant thermophysical properties, we can write Equations 6, 7, and 20 as

$$\frac{\tau_o}{N_R}\frac{\partial^2\theta_s}{\partial\tau^2}-2(1-\omega_o)(-Q^+-Q^-+2E_b)+\frac{N_c}{N_R}\frac{\partial\theta_g}{\partial\tau}=0 \tag{27}$$

$$\frac{\partial\theta_g}{\partial\tau}=-\frac{N_g}{\tau_o}(\theta_s-\theta_g) \tag{28}$$

Then, the governing equations become Equations 17, 18, 27, and 28. The solutions for θ_s, θ_g, Q^+, and Q^- can be obtained as functions of τ, the parameters τ_o/N_k, N_c/N_R, and N_g/τ_o. Recalling the definition of each parameter, we can express the parameter N_c/N_R as

$$\frac{N_c}{N_R}=\frac{m_g c_{pg}}{\sigma(T_1+T_2)(T_1^2+T_2^2)} \tag{29}$$

The parameter N_c/N_R does not include the thickness of the porous layer.

Figure 10 shows the solid temperature at the front surface for various parameters. We obtained the temperature numerically, using the same procedure as for Figure 9. The standard parameters are those given in Table 1 and $T_2=300$ K; the particle diameter varies from 10 μm to 1 mm. These results are plotted as solid lines. The radiation source temperature, T_1, is then set at 2,000 K in order for irradiation to be approximately 1 MW m^{-2} for each particle diameter. The very good correlation between these two source temperatures shows that the surface temperature is well described using the advection–radiation parameter, N_c/N_R, for a wide range of radiation source temperatures and mass fluxes.

The slope of the surface temperature versus N_c/N_R is steepest at about $1<N_c/N_R<2$, and the mass flux and the particle diameter are responsible for reducing the surface temperature in the region. However, either too large or too small mass fluxes (i.e., $N_c/N_R<0.3$ or $N_c/N_R>10$) do not affect the surface temperature greatly. Thus we can conclude that if we choose a mass flux so that N_c/N_R is between 1 and 2, the advective flux is comparable to the radiative flux, and advection cooling is very effective in the range of N_c/N_R larger than 1 or 2.

Conclusions

A theoretical investigation of an active thermal insulation system was performed in which the temperature dependence of thermophysical properties was taken into account for both nondissociating and dissociating gases. Air and hydrogen, pure ammonia, and ammonia at an equilibrium state were chosen as examples.

The constant-property solution based on the thermophysical properties evaluated at the inlet gas temperature agreed well with the variable-property solution, despite the large variation in thermophysical properties through the layer. Comparison between pure ammonia and ammonia at an equilibrium state for the same mass flux showed large differences in gas temperature. However, the difference in solid temperature distribution is relatively small.

If the advection parameter A, defined by Equation 25, for different gases is the same, the temperature distributions in the solids correlated well. The required mass flux of hydrogen is 14 times smaller than that of air, and the mass flux of ammonia is between these two extremes. So far as the molar flux of the gas is concerned, parameter A is approximately the same for the same molar flux of each monoatomic, diatomic, and polyatomic gas.

At the initial stage of heating, the thermal penetration depth is not affected by gas injection, and the depth is much larger than that for the case of pure conduction. With increasing time, the penetration depth with gas injection reaches a finite value of a few millimeters deep, and the heat flow through the layer is eliminated. However, the penetration depth without gas injection or for pure conduction increases monotonically with time.

For estimating the surface temperature, we introduced the advection–radiation parameter N_c/N_R, defined by Equation 29. If the advection–radiation parameter is larger than 1 or 2, advective cooling is effective. The mass flux that results in either a too-large or too-small advection–radiation parameter does not influence the surface temperature of the solid. The smaller particle diameter of the porous medium is more effective in protecting the structure. Not only effective cooling but also reliable and stable conditions are usually required for the thermal protection. Thus an analysis for optimizing criteria is recommended.

References

1 Sutton, G. P., Wagner, W. R., and Seader, J. D. Advanced cooling techniques of rocket engines. *Aero. and Astro.*, 1966, **4**, 60–71

2 Matthews, L. K., Viskanta, R., and Incropera, F. P. Combined conduction and radiation heat transfers in porous materials

heated by intense solar radiation. *J. Solar Energy Eng.*, 1985, **107**, 29–34
3 Yarbrough, D. W., Tong, T. W., and McElroy, D. L. Use of fine powders for high thermal resistance. *High Temp. Sci.*, 1985, **19**, 213–225
4 Chu, H. S., Stretton, A. J., and Tien, C. L. Radiative heat transfer in ultra-fine powder insulations. *Int. J. Heat Mass Transfer*, 1988, **31**, 1627–1634
5 Hartnett, J. P. Mass transfer cooling. *Handbook of Heat Transfer Applications*, 2nd ed. (W. M. Rohsenow, J. P. Hartnett, and E. N. Ganic, Ed.), McGraw-Hill, New York, 1985, 1-1–1-109
6 Echigo, R. High temperature heat transfer augmentation. *High Temperature Heat Exchangers* (Y. Mori, A. E. Sheindlin, and N. Afgan, Eds.), Hemisphere, Washington, DC, 1986, 230–259
7 Yoshizawa, Y., Echigo, R., and Tomimura, T. A study on a high performance radiant heater. *Proc. ASME/JSME Thermal Eng. Joint Conf.*, Vol. 5 (P. J. Marto and I. Tanasawa, Eds.), ASME/JSME, New York/Tokyo, 1987, 317–323
8 Flamant, G., Menigault, T., and Schwander, D. Combined heat transfer in a semitransparent multilayer packed bed. *J. Heat Transfer*, 1988, **110**, 463–467
9 Maruyama, S., Viskanta, R., and Aihara, T. Active thermal protection against intense irradiation. *J. Thermophys. Heat Transfer*, 1989, **3**, 389–394
10 Börsch-Supan, W., Hunter, L. W., and Kuttler, J. R. Endothermic gasification of a solid by thermal radiation absorbed in depth. *Int. J. Heat Mass Transfer*, 1984, **27**, 1171–1182
11 Gorton, R. L. An experimental study of ammonia as a reactive transpiration coolant—Porous body cooling. *J. Heat Transfer*, 1969, **91**, 561–567
12 Huber, M. L. and Jones, M. C. A frequency response study of packed bed heat transfer at elevated temperatures. *Int. J. Heat Mass Transfer*, 1988, **31**, 843–853
13 Aihara, T., Maruyama, S., and Choi, J. C. Laminar free convection with variable fluid properties in vertical ducts of different cross-sectional shapes. *Heat Transfer—1986*, Vol. 4 (C. L. Tien, V. P. Carey, and J. K. Ferrell, Eds.), Hemisphere, Washington, DC, 1986, 1581–1586
14 Kays, W. M. and London, A. L. *Compact Heat Exchangers*, 3rd ed., McGraw-Hill, New York, 1977, 88–89
15 Aihara, T. and Maruyama, S. Laminar free convective heat transfer in vertical uniform-heat-flux ducts (numerical solution with constant/temperature-dependent fluid properties). *Heat Transfer Japanese Res.*, 1986, **15**, 69–86
16 Menguc, M. P. and Viskanta, R. Comparison of radiative transfer approximations for a highly forward scattering planar medium. *J. Quant. Spectrosc. Radiative Transfer*, 1983, **29**, 381–394
17 Reiss, H. *Radiative Transfer in Nontransparent, Dispersed Media*, Springer-Verlag, Berlin, 1988, 136–138
18 Yaws, C. L. *Physical Properties*, McGraw-Hill, New York, 1977
19 Liquide, L. *Encyclopedie des Gaz*, Elsevier, Amsterdam, 1976, 964
20 Suris, A. L. *Handbook of Thermodynamic High Temperature Process Data*, Hemisphere, Washington, DC, 1987
21 Bird, R. B., Stewart, W. E., and Lightfoot, E. N. *Transport Phenomena*, John Wiley, New York, 1960, 19–26, 253–260
22 *JSME Data Book: Heat Transfer*, 4th ed. (K. Katayama, Ed.), Maruzen, Tokyo, 1986, 329
23 Kurosaki, Y., Takeuchi, M., Kashiwagi, T., and Yamada, J. Development of measuring method for radiative properties of fibrous porous media. *Proc. ASME/JSME Thermal Eng. Joint Conf.*, Vol. 4 (P. J. Marto and I. Tanasawa, Eds.), ASME/JSME, New York/Tokyo, 1987, 319–325
24 Matthews, L. K., Viskanta, R., and Incropera, F. P. Development of inverse methods for determining thermophysical and radiative properties of high-temperature fibrous materials. *Int. J. Heat Mass Transfer*, 1984, **27**, 487–495
25 Viskanta, R. and Menguc, M. P. Radiative transfer in dispersed media. *Appl. Mech. Rev.*, 1989, **42**, 241–259